Through The Flare: A* Algorithm for Radiation-Aware Satellite Trajectory Planning

Muhamad Hasbullah Faris – 18223014
Program Teknik Informatika
Sekolah Teknik Elektro dan Informatika
Institut Teknologi Bandung, Jalan Ganesha 10 Bandung
hasbullah4869@gmail.com, 18223014@std.stei.itb.ac.id

***Abstract*—This research employs the A* search algorithm to compute radiation-aware satellite trajectories that minimize cumulative proton flux exposure during Solar Energetic Particle (SEP) events. The algorithm searches a two-dimensional cost grid constructed from real NASA OMNI proton flux data, evaluating routes based on three core design choices. First, each grid cell carries a raw proton flux cost in particle flux units (pfu), preserving true radiation intensity rather than a normalized abstraction. Second, an admissible heuristic, the Euclidean distance to the goal scaled by the grid's minimum cell cost, guarantees that the path returned is optimal, with diagonal moves penalized by a $\sqrt{2}$ factor to preserve geometric distance. Third, performance is benchmarked against a simulated NASA threshold baseline, in which cells exceeding the NOAA S1 alert limit of 10 pfu are marked impassable and Breadth-First Search finds the shortest route with no cost optimization. Three solar activity scenarios are evaluated: quiet sun (January 2017), moderate activity (May–June 2017), and a major SEP event (September 2017, peak flux ≈566 pfu). Results show that A* consistently finds minimum-exposure trajectories across all scenarios, while the threshold baseline fails entirely during the SEP event, unable to find any passable route once the grid is mostly saturated above the danger threshold. This method not only minimizes radiation exposure but also exposes a structural limitation in current NASA operational practice, where treating radiation as a binary condition discards an entire dimension of optimization.**

***Keywords*—A* algorithm, satellite trajectory planning, solar energetic particles, radiation avoidance, NASA OMNI, space weather**

I. Introduction

For thousands of years, human civilization has pushed against the edges of what it knows. Oceans, deserts, and mountain ranges, often with no certainty of what waited on the other side. Space is simply the newest edge, and satellites are how much of that exploration now happens, invisible to the eye, doing the watching and reaching that ships once did.

However, that curiosity always come with a cost. Sailors lost ships to storms they could not predict, and early aviators lost their lives to weather they did not yet understand. In orbit, the equivalent danger is mostly invisible: it lives in particles, not waves, and is just as capable of ending a mission. Solar Energetic Particle (SEP) events, bursts of high-energy charged particles accelerated by solar flares and coronal mass ejections (CMEs), are one of the most persistent risks a satellite faces once it leaves the ground [2]. On September 6, 2017, an X9.3 solar flare, the most powerful in over a decade, triggered an SEP event with sustained proton flux above 500 pfu at energies greater than 10 MeV [3], causing anomalies on multiple operational satellites. Current operational responses are governed by NOAA Space Weather Prediction Center (SWPC) alert thresholds: once flux crosses the danger limit, operators place satellites into safe mode or defer maneuvers until the event subsides [4]. NASA's Space Radiation Analysis Group (SRAG) operates on a similar paradigm, one in which *"no actions are taken based on elevated likelihood of an SPE prior to an event occurring"* [5]. Wait it out, or shelter. There is no third option.

A satellite that must maneuver during a radiation event, for example to perform orbital maintenance, debris avoidance, or a rendezvous, has no formal method for choosing a path that minimizes how much radiation it absorbs along the way. The threshold-based framework treats radiation as binary: a cell is either safe or forbidden, and the spatial gradient of flux that persists even within nominally *safe* regions is ignored entirely. A*-based radiation-cost pathfinding has been explored in adjacent domains, such as minimizing dose exposure for personnel navigating nuclear emergency environments [8], but its application to satellite trajectory planning during SEP events remains unexplored.

Through this lens, this paper proposes treating radiation as a continuous cost instead. The A* algorithm searches a two-dimensional grid built from measured proton flux data, letting a satellite minimize total radiation exposure along its path. A simulated NASA threshold baseline, using Breadth-First Search through cells below the 10 pfu limit, serves as the comparator across three scenarios drawn from the NASA OMNI dataset: quiet sun, moderate activity, and the September 2017 SEP event.

II. A* Algorithm

A. Overview

A* is an informed best-first graph search algorithm first introduced by Hart, Nilsson, and Raphael in 1968 [1]. It is widely used in pathfinding and trajectory optimization due to its guarantee of optimality when the heuristic function is admissible and its practical efficiency over uninformed search methods such as Dijkstra's algorithm in large state spaces.

A* selects the next node to expand based on the evaluation function:

$$f(n) = g(n) + h(n) \tag{1}$$

where $g(n)$ is the actual accumulated cost from the start node to node n, and $h(n)$ is a heuristic estimate of the remaining cost from n to the goal. Nodes are maintained in a priority queue ordered by $f(n)$; the node with the lowest f value is expanded at each iteration.

B. Admissibility of the Heuristic

A heuristic is *admissible* if it never overestimates the true cost to reach the goal. For the radiation cost grid, we define:

$$h(n) = d_{\text{euclidean}}(n, \text{goal}) \times c_{\min} \tag{2}$$

where $d_{\text{euclidean}}$ is the straight-line distance in grid cells between node n and the goal, and $c_{\min}$ is the minimum cell radiation cost in the grid. Since the minimum cost along any path from n to the goal cannot be less than $c_{\min}$ per unit distance, $h(n)$ never overestimates and is therefore admissible, guaranteeing that A* returns an optimal path [1].

C. Edge Cost Model

The grid uses 8-connected movement. Edge costs account for diagonal traversal:

$$w(a, b) = \begin{cases} \phi(b) & \text{if } a \text{ and } b \text{ share an axis} \\ \sqrt{2} \cdot \phi(b) & \text{if movement is diagonal} \end{cases} \tag{3}$$

where $\phi(b)$ is the raw proton flux at cell b in pfu. The diagonal factor of $\sqrt{2}$ preserves geometric path length proportionality. The total path cost is the sum of all edge costs along the trajectory.

D. Pseudocode

Algorithm 1 A* for Radiation-Aware Trajectory Planning

Require: grid G, start s, goal t
Ensure: minimum-exposure path from s to t

```
Initialize open set O ← {s} as a min-heap on f
g[s] ← 0; f[s] ← h(s); parent[s] ← None
while O ≠ ∅ do
    n ← arg min_{x∈O} f(x); remove n from O
    if n = t then return reconstruct_path(parent, t)
    end if
    for each neighbor m of n in G do
        g' ← g[n] + w(n, m)
        if g' < g[m] then
            g[m] ← g'; f[m] ← g' + h(m)
            parent[m] ← n; add/update m in O
        end if
    end for
end while
return ∅                                  ▷ No path found
```

E. Complexity Analysis

Let V denote the number of cells in the grid and E the number of edges, where $E = O(V)$ for an 8-connected grid since each cell has at most 8 neighbors. The priority queue is implemented with a binary min-heap via `heapq`, giving $O(\log V)$ cost per insertion or extraction.

Time complexity. In the worst case, A* visits every node and relaxes every edge once, giving a bound identical in form to Dijkstra's algorithm [7]:

$$T(V, E) = O\big((V + E) \log V\big) \tag{4}$$

For the 50×50 grid used in this study, $V = 2500$ and $E \leq 8V = 20000$, giving a worst-case bound of approximately $O(2.25 \times 10^5 \cdot \log_2 2500) \approx O(2.5 \times 10^6)$ priority-queue operations. In practice, A* terminates far earlier than this bound because the admissible heuristic from Equation (2) prunes nodes whose $f(n)$ value cannot improve on the current best estimate. This is reflected empirically in Table II, where A* expands 968–1504 nodes against the $V = 2500$ worst case, roughly a 40–60% reduction.

A* maintains the open set, a closed set or equivalent visited record, and a g-cost and parent pointer per visited node. Each of these structures scales with the number of nodes stored, giving:

$$S(V) = O(V) \tag{5}$$

For the 2500-cell grid, this is a small and fixed memory footprint regardless of scenario, since the grid dimensions, not the radiation intensity, determine the state space size.

The NASA threshold baseline uses Breadth-First Search, which shares the same $O(V+E)$ time and $O(V)$ space bounds without the $\log V$ priority-queue factor, but without heuristic guidance it cannot prioritize promising directions and instead expands nodes in strict distance order from the start. This is why the NASA threshold baseline frequently expands close to the full $V = 2500$ nodes even on the quiet sun scenario, despite ultimately failing to optimize the path it returns.

III. Solar Energetic Particles and Space Weather

Solar Energetic Particle (SEP) events are bursts of high-energy charged particles, predominantly protons, electrons, and heavy ions, accelerated to near-relativistic velocities by solar flares and coronal mass ejections (CMEs) [2]. Two distinct acceleration mechanisms are recognized. Impulsive events are driven by magnetic reconnection in solar flares, producing particle-rich but short-duration bursts confined to narrow angular extents. Gradual events, which produce the most hazardous conditions for satellite operations, are driven by CME-driven interplanetary shocks that can accelerate protons over extended periods and fill large volumes of the inner heliosphere with high-energy particles.

The integral proton flux at energies greater than 10 MeV is the standard operational quantity for SEP monitoring, as protons at these energies carry sufficient energy to penetrate satellite shielding and deposit ionizing dose in sensitive electronics. The NOAA S-scale classifies radiation storm severity

in five levels (S1 to S5) based on this flux channel, with S1 triggered at 10 pfu and S5 at 100,000 pfu [4].

A. Effects on Satellite Systems

High-energy protons interact with satellite electronics through two primary damage mechanisms. Single-Event Effects (SEEs) occur when a single particle traverses a sensitive volume, depositing sufficient charge to flip a memory bit, trigger a latch-up, or cause a logic error. These effects are stochastic and can occur even during moderate flux elevations. Total Ionizing Dose (TID) accumulates over a satellite's lifetime as particles deposit energy in semiconductor oxides, gradually degrading transistor performance and ultimately causing component failure [2]. During major SEP events, SEE rates can increase by several orders of magnitude, making continued operation of unshielded payloads inadvisable.

B. The September 2017 SEP Event

The September 2017 period produced the most intense SEP conditions in over a decade. On September 4, an X2.2 solar flare initiated the first moderate particle flux increase of the period. Two days later, on September 6, an X9.3 flare, launched a fast CME that drove an interplanetary shock into the inner heliosphere. The shock accelerated protons to high energies over the following 24 hours, producing an S3 (Strong) radiation storm with peak integral proton flux exceeding 566 pfu at energies above 10 MeV on September 7–8, as recorded in the NASA OMNI dataset [3].

The temporal evolution of this event is directly captured in the radiation grid used in this study. DOY 244–248 (September 1–5) represent the pre-flare quiet window. DOY 249–253 (September 6–10) represent the onset and peak of the storm. DOY 254–273 represent the gradual decay phase. This rise-peak-decay structure makes the September 2017 event a strong test case for radiation-aware trajectory planning: the grid contains both navigable corridors and fully saturated danger zones within a single 30-day window.

IV. Data and Grid Construction

A. Dataset

The proton flux data used in this study is drawn from the NASA OMNI dataset [6], accessed via the NASA Goddard Space Flight Center OMNI Web interface. The selected variable is the integral proton flux at energies greater than 10 MeV, reported at one-hour temporal resolution. This channel is the standard reference for operational SEP event monitoring under the NOAA S-scale classification.

Three time periods are selected to represent distinct solar activity regimes:

- **Quiet sun:** January 1–31, 2017 (DOY 1–31). Background flux ranging approximately 0.15–0.21 pfu. No significant solar activity.
- **Moderate activity:** May 27 – June 2, 2017 (DOY 147–155). Mild flux elevation in the range 0.14–0.25 pfu, corresponding to low-level solar wind perturbations.
- **SEP event:** September 1–30, 2017 (DOY 244–273). Peak flux of approximately 566 pfu recorded on September 7–8, following the X9.3 solar flare of September 6. This event produced an S3 (Strong) radiation storm classification under the NOAA S-scale.

Fill values of 9999.99 in the OMNI dataset, indicating missing measurements, are filtered prior to grid construction.

B. Grid Construction

Each time series is mapped to a 50×50 two-dimensional grid representing a simplified orbital plane. The 2,500 hourly flux measurements from each scenario are reshaped using column-major (Fortran) ordering, such that grid rows correspond to time-indexed altitude bands and columns correspond to angular orbital position. Cell values retain their raw pfu units.

The grid is fully connected with 8-directional movement. Each cell carries a radiation cost equal to its raw proton flux value. The three start-goal pairs used in all experiments are:

- Pair 0: $(0, 0) \rightarrow (49, 49)$
- Pair 1: $(0, 49) \rightarrow (49, 0)$
- Pair 2: $(5, 5) \rightarrow (44, 44)$

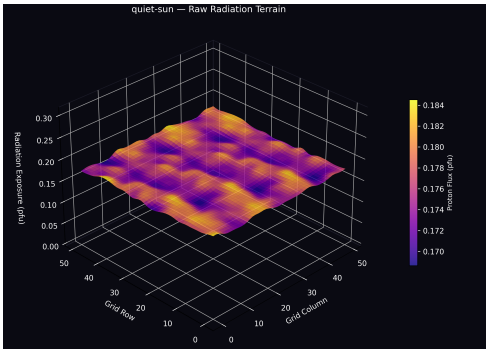

Fig. 1. Raw radiation terrain — quiet sun (January 2017). Proton flux values range from 0.15 to 0.21 pfu with negligible spatial variation.

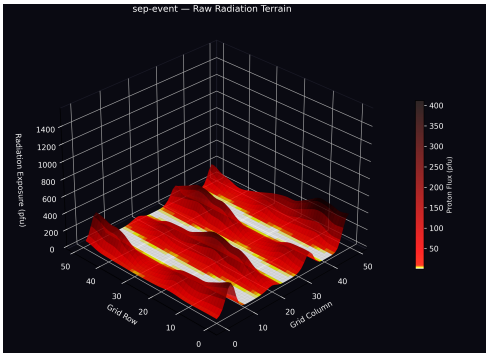

Fig. 2. Raw radiation terrain — SEP event (September 2017). Peak flux exceeds 500 pfu, producing pronounced radiation mountains spanning multiple grid sectors.

V. Proposed Method

A. Framework Overview

The proposed framework models satellite trajectory planning as a weighted graph search problem on the radiation cost grid. Given a start and goal cell, A* is invoked to find the path that minimizes total accumulated proton flux exposure, defined as the sum of edge costs along the path as in Equation (3). Figure 3 summarizes the end-to-end pipeline, from raw NASA OMNI measurements through grid construction, parallel path search by A* and the NASA threshold baseline, to the final exposure comparison reported in Section VI.

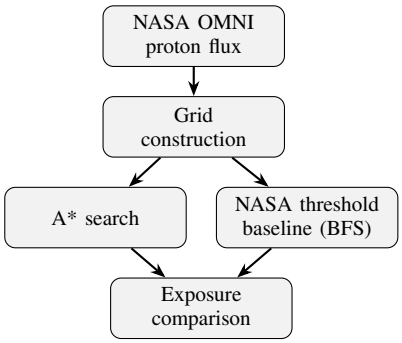

Fig. 3. End-to-end pipeline. Raw proton flux measurements are reshaped into a 50×50 cost grid, then searched in parallel by A* and the NASA threshold baseline. Resulting paths are compared on total exposure, path length, nodes expanded, and runtime.

B. NASA Threshold Baseline

The operational threshold-based approach is implemented as a direct comparator. Following NOAA SWPC S1 alert criteria [4], all grid cells with raw flux exceeding 10 pfu are marked as impassable. Breadth-First Search is then applied to find the geometrically shortest path through the remaining passable cells, with no cost optimization. The baseline makes no attempt to minimize radiation exposure along the chosen route; it only avoids cells above the binary threshold.

Results for this baseline, are reported numerically in the result tables of Section VI rather than overlaid on the radiation terrain figures.

C. Key Distinction

The fundamental difference between the two approaches is illustrated in Table I. A* treats radiation as a continuous cost landscape and minimizes exposure throughout the trajectory. The threshold baseline treats radiation as binary and applies no optimization beyond threshold enforcement.

TABLE I. Comparison of Trajectory Planning Approaches

Property	A*	NASA Threshold
Cost model	Continuous gradient	Binary safe/blocked
Optimization	Minimum exposure	Shortest passable path
Heuristic	Admissible $h(n)$	None
Handles SEP event	Always finds path	Fails if grid saturated
Optimality guarantee	Yes	No

VI. Experiment and Results

A. Setup

All experiments are implemented in Python 3.10. The priority queue uses Python's `heapq` standard library module. Each of the three start-goal pairs is evaluated on each of the three radiation scenarios for both A* and the NASA threshold baseline, yielding 18 runs in total. Metrics recorded per run are: total radiation exposure (pfu), path length (cells), nodes expanded, and execution time (ms).

B. Results

TABLE II. Results — Quiet Sun (January 2017)

Algo.	P	Exp. (pfu)	Len.	Nodes	ms
A*	0	11.97	52	1373	13.630
NASA Threshold	0	12.11	50	2500	7.886
A*	1	12.01	51	1504	14.972
NASA Threshold	1	12.16	50	2451	7.649
A*	2	9.40	42	968	8.909
NASA Threshold	2	9.52	40	2025	6.134

TABLE III. Results — Moderate Activity (May–Jun 2017)

Algo.	P	Exp. (pfu)	Len.	Nodes	ms
A*	0	12.10	52	1524	14.782
NASA Threshold	0	12.28	50	2500	8.248
A*	1	12.08	52	1458	15.428
NASA Threshold	1	12.09	50	2451	7.536
A*	2	9.63	42	1141	11.077
NASA Threshold	2	9.76	40	2025	6.200

TABLE IV. Results — SEP Event (September 2017)

Algo.	P	Exp. (pfu)	Len.	Nodes	ms
A*	0	685.48	135	2303	20.209
NASA Threshold	0	—	—	97	0.300
A*	1	1605.28	108	2174	19.857
NASA Threshold	1	—	—	0	0.022
A*	2	376.58	70	1744	15.627
NASA Threshold	2	—	—	0	0.016

— no path found; grid saturated above 10 pfu.

C. Discussion

During low-activity periods, all grid cells fall below the 10 pfu threshold, rendering every cell passable for the baseline. Under these conditions, both A* and the NASA threshold baseline produce valid paths. A* selects near-straight diagonal trajectories, confirming that deviating from the shortest path incurs unnecessary additional exposure when the radiation landscape is spatially uniform. The NASA baseline's shortest-path approach yields a longer total exposure than A* due to the absence of any cost-minimization step, as the baseline selects minimum steps rather than minimum flux.

The September 2017 scenario produces the sharpest divergence between the two approaches. Raw proton flux at peak

exceeds 566 pfu, with the 10 pfu threshold falling at approximately the 1.7th percentile of the grid's flux distribution. Consequently, over 98% of grid cells are marked impassable by the threshold method. The NASA threshold baseline fails to find any continuous path for all three start-goal pairs, as shown in Tables II–IV (marked "—"). A*, by treating radiation as a continuous cost rather than a binary barrier, identifies low-flux corridors corresponding to temporal windows before the September 6 flare onset (DOY 244–248), navigating the grid to deliver a minimum-exposure trajectory.

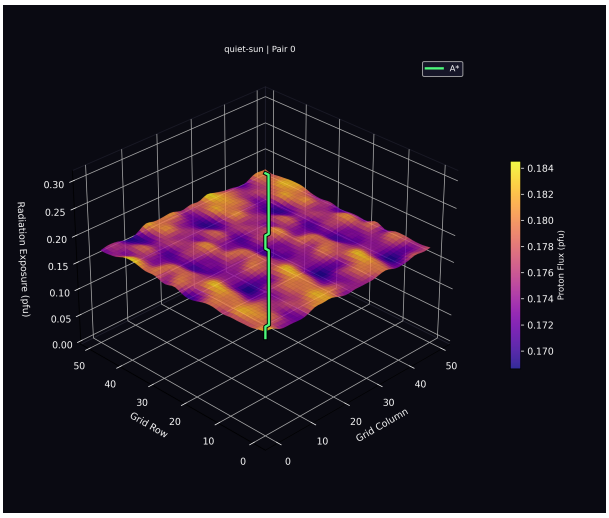

Fig. 4. Quiet sun scenario, Pair 0.All cells are below the 10 pfu threshold. A* selects a near-straight trajectory minimizing total flux.

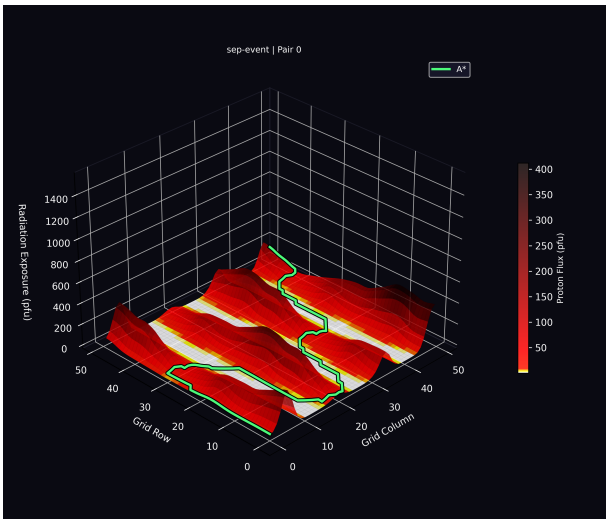

Fig. 5. SEP event scenario, Pair 0. Red/dark zones indicate cells exceeding the 10 pfu danger threshold. A* (gold) navigates through low-flux corridors in the pre-flare temporal window.

The results suggest two complementary roles for A* in satellite operations. First, during moderate conditions, A* provides continuous exposure optimization that the threshold method does not, potentially reducing cumulative total ionizing dose over extended mission lifetimes. Second, and more critically, during major SEP events where the threshold method provides no guidance, A* retains the ability to produce actionable trajectories. This matters most for satellites that cannot afford to hold indefinitely, such as those performing time-critical rendezvous or debris avoidance maneuvers.

D. Limitations

Three simplifications bound the scope of this study. First, the grid represents a two-dimensional orbital plane rather than true three-dimensional orbital mechanics; real trajectory planning must also account for orbital velocity, fuel budget, and orbital period constraints that are not modeled here. Second, the mapping from hourly time-series flux measurements to spatial grid coordinates is a modeling convenience applied via Fortran-order reshaping; it preserves the relative cost structure needed for path comparison, but the resulting spatial layout is illustrative rather than an empirically measured flux gradient across orbital positions. Third, the NASA threshold baseline implemented here is a simplified simulation of the NOAA S1 alert criterion, not the literal NASA SRAG decision process, which in practice may weigh mission criticality, instrument sensitivity, and predicted event duration alongside the flux threshold. These simplifications are appropriate for isolating the algorithmic contribution of cost-aware search, but a deployment-ready system would need to address all three.

VII. Conclusion

This paper proposed and evaluated a radiation-aware satellite trajectory planning framework based on the A* search algorithm applied to a proton flux cost grid derived from NASA OMNI measurements. Experiments across three solar activity scenarios (quiet sun, moderate activity, and the September 2017 SEP event) show that A* consistently produces minimum-exposure paths, while the NOAA threshold-based approach fails entirely once the grid is mostly saturated above the safety threshold.

The key contribution is reframing radiation avoidance from a binary safe/blocked decision into a continuous cost-minimization problem. This makes trajectory optimization possible across the full range of solar activity, instead of deferring every decision to reactive threshold monitoring. The admissible heuristic in Equation (2) guarantees path optimality, and using real flux data from a documented event means the evaluation is tied to an actual recorded SEP event rather than a synthetic scenario.

Future work could extend this framework to three-dimensional orbital mechanics built on actual orbital position data rather than a reshaped time series, fold in real-time GOES flux feeds for dynamic re-planning, and check the resulting paths against recorded satellite maneuver logs from the September 2017 period. The cost function itself could also be generalized into a multi-objective formulation that weighs radiation exposure against fuel cost or delta-v, giving operators a tunable trade-off rather than a single fixed objective. Finally, following the organ-specific dose modeling used by Li et al. [8] in terrestrial radiation environments, instrument-specific

sensitivity weighting could replace the flat flux-based cost used here, accounting for the fact that not every onboard component is equally vulnerable to the same radiation dose.

REFERENCES

[1] P. E. Hart, N. J. Nilsson, and B. Raphael, "A formal basis for the heuristic determination of minimum cost paths," *IEEE Trans. Syst. Sci. Cybern.*, vol. 4, no. 2, pp. 100–107, 1968. doi: 10.1109/TSSC.1968.300136

[2] D. V. Reames, "Particle acceleration at the sun and in the heliosphere," *Space Sci. Rev.*, vol. 90, pp. 413–491, 1999. doi: 10.1023/A:1005105831781

[3] G. A. de Wasseige et al., "The September 2017 SEP events as observed by INTEGRAL/SPI," *J. Space Weather Space Clim.*, vol. 9, p. A27, 2019. doi: 10.1051/swsc/2019024

[4] NOAA Space Weather Prediction Center, "Space weather scales: Radiation storms (S-scale)," [Online]. Available: https://www.swpc.noaa.gov/noaa-scales-explanation [Accessed: Jun. 2025]

[5] NASA Space Radiation Analysis Group, "ISS Crew Radiation Protection: ConOps and Operational Constraints," NASA Johnson Space Center Technical Document, Houston, TX, 2014.

[6] J. H. King and N. E. Papitashvili, "Solar wind spatial scales in and comparisons of hourly Wind and ACE plasma and magnetic field data," *J. Geophys. Res.*, vol. 110, A02104, 2005. doi: 10.1029/2004JA010649

[7] E. W. Dijkstra, "A note on two problems in connexion with graphs," *Numer. Math.*, vol. 1, pp. 269–271, 1959. doi: 10.1007/BF01386390

[8] Y.-C. Li, Z.-H. Yang, H. Tian, Z.-Y. Li, Q.-C. Huo, G.-M. Sun, S.-P. Wang, Q. Chen, J. Fu, and G.-H. Tao, "A three-dimensional space path planning method based on A* algorithm in radiation environment," *Ann. Nucl. Energy*, 2025. [Online]. Available: https://www.sciencedirect.com/science/article/abs/pii/S0149197025004408

VIDEO LINK AND ATTACHMENT

Video: https://youtu.be/9qplMjnN9Ms

GitHub Link: https://github.com/hsbu/through-the-flare

ACKNOWLEDGEMENT

The author expresses gratitude to God Almighty for the strength and clarity to complete this work. Sincere thanks are extended to the lecturers of IF2211 Strategi Algoritma for their guidance throughout the semester, to family for their unwavering support, and to fellow students of Sistem dan Teknologi Informasi ITB 2023 for the shared struggle and encouragement. The author is also grateful to the writer of a previous semester's standout paper in this course, whose work served as a quiet benchmark throughout a difficult semester and a standard the author hoped to rise to meet.

STATEMENT

I hereby declare that this paper is my own original writing, not an adaptation or translation of another person's paper, and not plagiarized.

Bandung, June 19, 2026

Muhamad Hasbullah Faris – 18223014